Supplementary Material to
Enhancing Drone Endurance in Sub-Zero Environments via Multi-Modal Bio-Chemical Approaches

Anirudh S - Grade XII - Shraddha Children's Academy, Chennai, India
Arnav Venkatesh - Grade XII - NHVPS RR Nagar, Bangalore, India

Abstract

This supplementary material provides extended data and justification material for the main project. It contains: (i) a parameter table with measured and literature-sourced values used by the simulations, (ii) stepwise derivations of the model equations used in the study, (iii) full Python model outputs, (iv) high-resolution renders and CAD links for the penguin-inspired propeller prototypes, and (v) ANSYS simulation inputs and settings used for the CFD simulation. The document is intended to allow reproducibility and to provide additional evidence underlying the claims in the main manuscript.

Contents

Note on scope

This Supplementary Material selectively presents additional information that supports the analyses in the main manuscript. Only the items necessary to reproduce or justify the main results are included here.

1 Parameter Values Used

Table 1: Parameter values used in the code, along with sources and estimate justifications.

Variable	Short description	Min Real	Max Real	Real (avg.)	Source
m_batt_kg (kg)	Battery mass.	0.045	0.468	0.120	[1, 2]
cp_batt (J/kg·K)	Battery specific heat capacity.	800	1100	950	[2]
T0_C (°C)	Initial battery temperature.			20	
T_ambient_C (°C)	Ambient / cold-chamber temperature.			−20	
h_W_m2K (W/m²·K)	Convective heat-transfer coefficient (battery enclosure).			40	[3, 4, 5]
A_m2 (m²)	External surface area of battery enclosure (estimate from physical pack size).			0.013	[6]
P_elec_W (W)	Electrical heat / constant power loss (electronics).			10	[7]
dt_s (s)	Simulation timestep.			1.0	
tmax_s (s)	Simulation duration (battery cell).			1200	
Q0_J (J)	Heater total energy (parameter used by heater model).			10000	[8](taken as an estimate that lies close that of hand warmers and military MRE, as specific values were not found)
tau_s (s)	Heater time constant.			600	
m_pcm_kg (kg)	PCM mass (chosen).			0.10	
cp_pcm (J/kg·K)	PCM sensible specific heat.			2000	[9]
L_pcm_Jperkg (J/kg)	PCM latent heat of fusion.			175000	[9]
Tm_C (°C)	PCM phase-change (melting) temperature.			0.0	[9]
delta_T (°C)	Half-width of PCM melting plateau.			1.5	[9]
LWC_g_m3 (g/m³)	Liquid water content (LWC).	0.01	1.2	0.6	[10]
V_rel_m_s (m/s)	Relative velocity at blade (impact speed, general UAV value).			15	(choice/estimate)
A_imp_m2 (m²)	Impingement area per blade.			0.04	(estimate for 9-inch prop)
eta_imp (–)	Impingement efficiency.			0.5	(estimate, derived below*)
T_surface_C (°C)	Surface temperature (freezing fraction calc).			−5.0	(choice/estimate)
droplet_diameter (µm)	Droplet diameter (for freezing calc).			20	[11]
adhesion_coeff baseline (–)	Baseline adhesion coefficient .			1.0	(≈100% ice sticks)
shedding_rate baseline (s^{-1})	Baseline shedding rate.			0.001	(very low for baseline props)
adhesion_coeff penguin (–)	Penguin-inspired adhesion coefficient .			0.25	≈25% ice sticks; a conservative scaling from [12]
shedding_rate penguin (s^{-1})	Penguin-inspired shedding rate .			0.01	(higher, icephobic) [12]
T0_N (N)	Baseline thrust (no ice).			3.8	(as per early ANSYS sims)
alpha (–)	Thrust mapping factor (T = T0·(1 - α·m_ice/m_ref)).			0.7	(Inferred from the ≈ 50% thrust reduction at ≈ 7 g ice accretion reported for small UAV rotors by[13])
m_ref_kg (kg)	Reference ice mass .			0.01	(arbitrary and can be swept for sensitivity)
t_final_s (s)	Simulation final time (icing sim).			1200	
rho_air (kg/m³)	Air density.			1.225	
LWC_list (g/m³)	LWC sweep values.			[0.1, 0.5, 0.6, 1.0]	
Tsurf_list (°C)	Surface temperature sweep values.			[−40, −25, −10, −2, 0, 2]	

*The impingement efficiency ($\eta_{\text{imp}} = 0.5$) was estimated from the Stokes-number correlation of Langmuir and Blodgett(1946)[14] for 20 μm droplets at 15 m/s over a 2 cm-scale surface. Using

$$St = \frac{\rho_d D_d^2 U}{18 \mu L_c},$$

with $\rho_d = 1000$ kg/m^3, $D_d = 2 \times 10^{-5}$ m, $\mu = 1.8 \times 10^{-5}$ Pa s, $U = 15$ m/s, and $L_c = 0.02$ m, gives $St \approx 0.46$. Applying the empirical correlation

$$\eta_{\text{imp}} \approx \frac{St}{St + 0.5},$$

yields $\eta_{\text{imp}} \approx 0.48$, rounded to 0.5 in this study. This lies within the 0.3–0.6 range reported for small-scale UAV stagnation regions [15] [14].

2 Derivations of Important Equations

Notation summary

Thermal model: m (battery mass), c_p (specific heat), h (convective coefficient), A (surface area), T, T_∞ (battery and ambient temperature), P_{elec} (electrical loss), Q_{chem} (chemical heater power).

Icing model: LWC (liquid water content), V_{rel} (relative velocity), A_{imp} (impingement area), η_{imp} (impingement efficiency), $\dot{m}_{\text{imp}}$ (mass flux), m_{ice} (ice mass).

Thrust mapping: T_0 (clean thrust), α (thrust sensitivity), m_{ref} (reference ice mass).

Detailed parameter definitions and values are listed in the main parameter table (Section 1).

Equation 1: Battery lumped thermal energy balance

Starting from the first law of Thermodynamics(energy conservation) for the battery control mass:

$$\text{rate of change of internal energy} = \text{input power} - \text{output power}.$$

Which is essentially that the energy stored inside the battery changes only because of power entering or leaving it. With a lumped-capacitance (uniform temperature) assumption, internal energy change is $mc_p \frac{dT}{dt}$. Inputs are electrical loss P_{elec} and chemical heater power $Q_{\text{chem}}(t)$. Output is the convective cooling to the ambient environment that is modeled using Newton's Law of Cooling: $hA(T - T_\infty)$. Writing signs so heating is positive:

$$mc_p \frac{dT}{dt} = P_{\text{elec}} + Q_{\text{chem}}(t) - hA(T - T_\infty).$$

as used in the model.

Notes on assumptions: uniform battery temperature (lumped model) and convectional external heat loss. PCM inclusion is handled in the model by modifying c_p locally near the phase-change temperature.

Equation 2: Chemical heater power model

We model the chemical heater as a finite energy source that releases a total energy Q_0 over time, following an exponential decay of instantaneous power. This provides a simple, first-order representation of exothermic chemical heat release.

Mathematical formulation:

We assume that the rate of heat release is proportional to the remaining energy content,

$$\frac{dQ}{dt} \propto -Q(t)$$

which leads to an exponential decay form upon integration:

$$Q(t) = Q_0 e^{-t/\tau}$$

where Q_0 is the total stored chemical energy (J), and τ is the characteristic time constant (s).

Differentiating with respect to time gives the instantaneous heat release rate (power output):

$$\dot{Q}_{\text{chem}}(t) = -\frac{dQ}{dt} = \frac{Q_0}{\tau} e^{-t/\tau}$$

Here, the prefactor Q_0/τ ensures that the total energy released over time equals Q_0.
Energy conservation check:

$$\int_0^\infty \dot{Q}_{\text{chem}}(t)\,dt = \int_0^\infty \frac{Q_0}{\tau} e^{-t/\tau}\,dt = Q_0$$

Parameter interpretation:

- Q_0: Total energy released (J).
- τ: Characteristic time constant of decay (s).
- At $t = 0$, the heater releases maximum power: $\dot{Q}_{\text{chem}}(0) = Q_0/\tau$.
- As $t \to \infty$, $\dot{Q}_{\text{chem}}(t) \to 0$.

Relevance to this project:
Real chemical heaters, such as exothermic salt-packs or catalytic heat sources, exhibit high initial heat flux that gradually declines as the reaction proceeds [16, 17]. The exponential decay form captures this physical trend while preserving total energy and using a single tunable parameter. It provides a realistic yet computationally light model for system-level UAV thermal analysis.
Limitations:

- Real heaters often display multi-stage kinetics (induction, rise, plateau, decay), not a pure exponential form.
- Temperature dependence of reaction rate (Arrhenius-type behavior) is neglected.
- A single time constant cannot fully represent multiple concurrent decay processes.
- Perfect heat transfer to the UAV components is assumed, neglecting ambient or structural losses.

Final form:

$$\dot{Q}_{\text{chem}}(t) = \frac{Q_0}{\tau} e^{-t/\tau}$$

This serves as a physically consistent and energy-conserving surrogate for real chemical heat sources, suitable for the UAV sub-zero environment model.

Equation 3: Droplet impingement mass flux (ice accretion input)

Consider a freestream containing liquid water (LWC: mass of liquid water per unit volume). The volume of air swept per second across the impingement area A_{imp} at relative speed V_{rel} is $V_{\text{rel}}\,A_{\text{imp}}$ ($\text{m}^3\,\text{s}^{-1}$). Multiplying by the LWC gives the mass flow of liquid water entering the impingement region per second. Not all of this mass necessarily sticks; an impingement efficiency η_{imp} accounts for fraction that actually impacts and remains available for freezing/collection. Thus:

$$\dot{m}_{\text{imp}} \;=\; \text{LWC} \cdot V_{\text{rel}} \cdot A_{\text{imp}} \cdot \eta_{\text{imp}}.$$

Written as the model equation used in the notebook:

$$\dot{m}_{\text{imp}} \;=\; \text{LWC}\; V_{\text{rel}}\; A_{\text{imp}}\; \eta_{\text{imp}}. \tag{1}$$

Notes: Freezing fraction and adhesion then convert this impinged mass flux into adhered ice mass $\dot{m}_{\text{ice}}$ used in the thrust surrogate.

Equation 4: Thrust degradation model under icing

This relationship models how ice accumulation reduces rotor thrust. The formulation is empirical, based on the assumption that thrust decreases approximately linearly with the amount of ice accreted on the blade. This assumption is taken to prevent code complexity as ANSYS CFD will handle it in a more realistic way; although results of both the code and CFD showed decreasing thrust with increase in amount of ice as explained in the main paper.

Baseline condition:

Let T_0 denote the clean thrust with no ice present:

$$T = T_0 \quad \text{when} \quad m_{\text{ice}} = 0$$

Linear degradation with ice mass:

We assume thrust reduction is proportional to the accumulated ice mass[18][19]. A proportionality constant α is introduced to represent how strongly ice affects thrust, relative to a reference ice mass m_{ref}:

$$\text{Fraction of thrust remaining} = 1 - \alpha \frac{m_{\text{ice}}}{m_{\text{ref}}}$$

where

- m_{ice}: current ice mass on the blade (kg)
- m_{ref}: reference ice mass corresponding to full thrust degradation (kg)
- α: empirical scaling coefficient (dimensionless)

Combine with baseline thrust:

Multiplying the fractional thrust remaining by the clean thrust gives:

$$T = T_0 \left(1 - \alpha \frac{m_{\text{ice}}}{m_{\text{ref}}}\right)$$

Physical constraint:

Thrust cannot be negative; once ice accumulation reaches a critical level, the model clips at zero:

$$T = T_0 \cdot \max\left(0, 1 - \alpha \frac{m_{\text{ice}}}{m_{\text{ref}}}\right)$$

Closing notes on assumptions

- **Thermal model (Eq1):** Assumes a lumped-capacitance system, i.e., uniform internal temperature. Spatial temperature gradients within the battery are neglected for simplicity, and convection to ambient is modeled via Newton's law of cooling. The PCM effect is included implicitly through a variable $c_p(T)$ near the phase-change region.
- **Chemical heater (Eq2):** Treated as a first-order exponential decay process releasing a total energy Q_0. This surrogate captures realistic transient heat flux without requiring full reaction kinetics. It neglects multi-stage reaction behavior and temperature feedback on reaction rate for simplicity purposes.
- **Impingement model (Eq3):** Assumes uniform liquid water content and constant impingement area exposed to flow. The efficiency η_{imp} represents an average over surface and droplet size distribution. Non-uniform droplet fluxes or 3D geometry effects are neglected for simplicity.
- **Thrust model (Eq4):** Employs a simple linear reduction of thrust with accumulated ice mass, clipped at zero. This is a surrogate mapping for faster simulations.

3 Python Model Results and Outputs

All simulation outputs (CSV and JSON) and additional generated figures are available at the following link:

Download python_outputs.zip (Google Drive link)

The archive contains all numerical results corresponding to the Colab notebook,

Some of the main plots/images are shown below for reference.

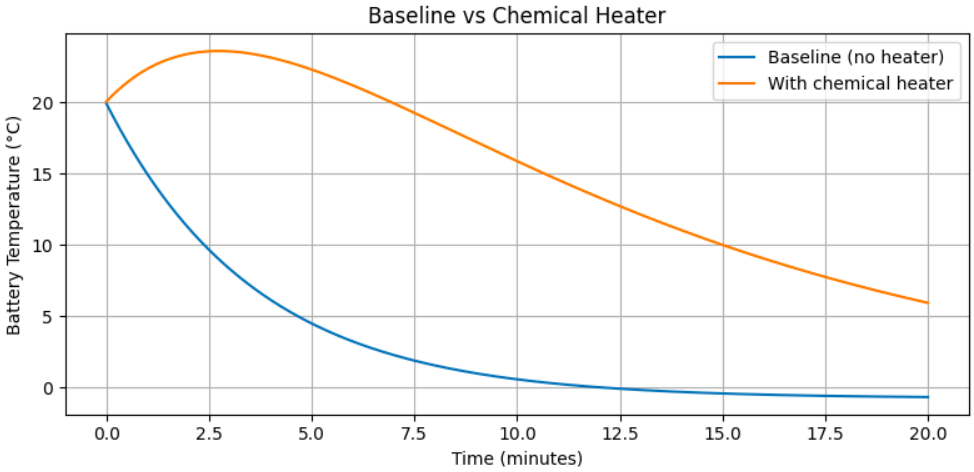

Figure 1: Comparison of battery temperature over time between baseline (no heater) and chemical heater-assisted configurations. The heater significantly slows the cooling rate, maintaining operational temperatures longer under sub-zero conditions.

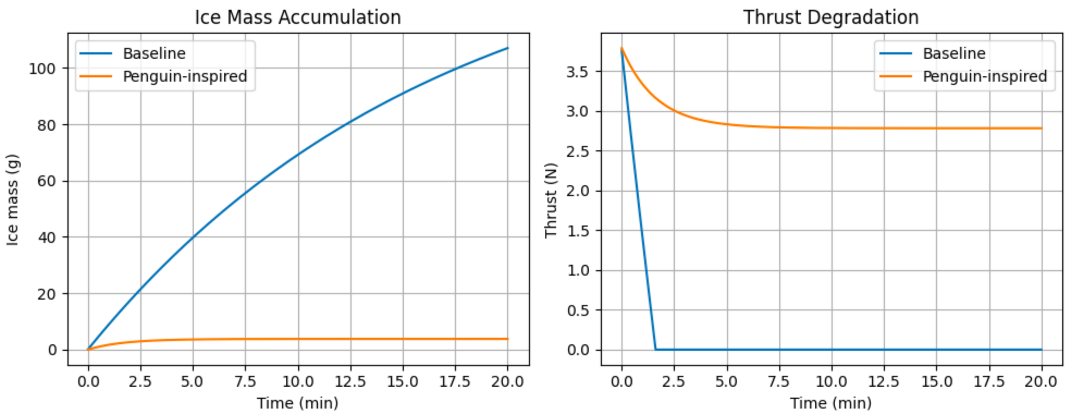

Figure 2: Icing and thrust degradation comparison between baseline and penguin-inspired surfaces. The penguin-textured coating shows drastically reduced ice accretion and improved sustained thrust. The thrust–ice coupling here is represented by a simplified linear relation

$$T = T_0 \left(1 - \alpha \frac{m_{\text{ice}}}{m_{\text{ref}}}\right),$$

where m_{ref} denotes the notional ice mass causing full thrust loss. This linear formulation is used only to illustrate relative degradation trends due to icing, not to predict aerodynamic losses. The sharp thrust reduction seen in baseline cases is therefore qualitative; more realistic aerodynamic effects are analyzed separately in the ANSYS CFD study.

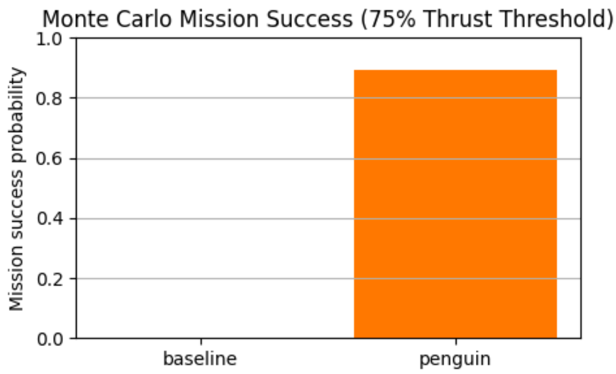

Figure 3: Monte Carlo simulation estimating mission success probability. A run was considered successful if thrust remained above 75% T_0 for at least 95% of the mission duration or at mission end, ensuring robustness against transient drops while maintaining the same 25% safety margin. The penguin-inspired design shows a higher likelihood of mission completion.

4 3D Models for Penguin-Feather Prop

Based on our research on penguin feather microstructure and its natural ice-shedding characteristics (as discussed in the main paper), several 3D prototypes were modelled to replicate these surface textures on drone propellers. The full set of CAD/3D models and design files is available at the link below:

Download 3D Model Prototypes (Google Drive link)

Multiple prototypes were developed to explore micro-texture spacing, curvature, and layering effects. Due to the high-resolution geometry, certain files are large and may not open reliably in lightweight viewers. It is recommended to view them using **Onshape**, **Autodesk Fusion 360** or **Blender** for compatibility and rendering accuracy.

Some renders of the models are shown below for reference.

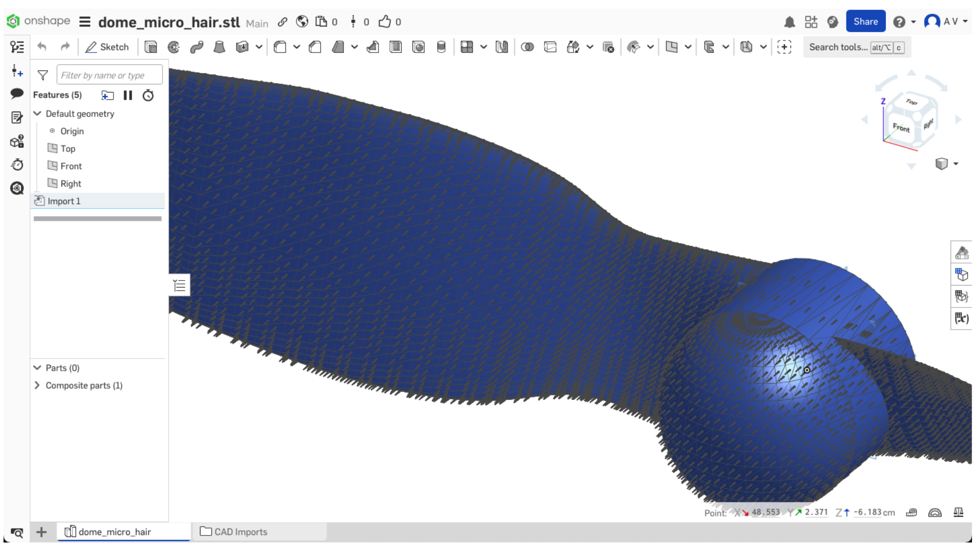

Figure 4: Propeller prototype featuring micro-hair structures that replicate the fine filament like texture of penguin feather barbs. This configuration increases surface roughness at the micro-scale(representative), promoting air entrapment and minimizing water adhesion during icing conditions.

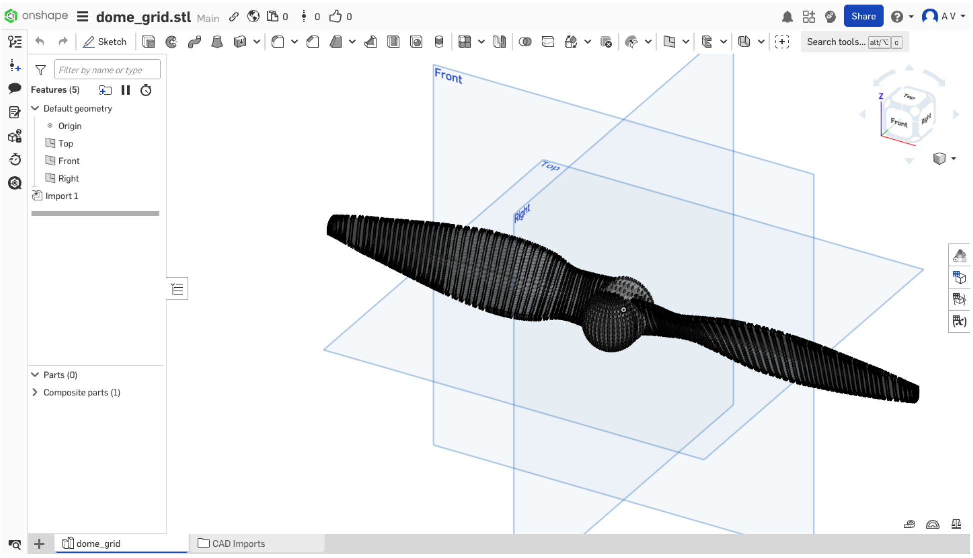

Figure 5: Alternate propeller prototype using a grid- or scale-patterned surface inspired by overlapping feather arrangements. This structure enhances ice detachment by creating discontinuities in the ice layer, improving passive anti-icing performance as discussed in the main paper.

5 ANSYS Simulation Files and Settings

All ANSYS Fluent and Workbench simulation files used for the ice accretion and aerodynamic performance analyses are available here:

Download ANSYS Simulation Files(Google Drive Link)

These include the Workbench project files (`.wbpj`), CAD file (`.iges`), and relevant FENSAP-ICE files.

Fluent Simulation Settings:

- **Propeller rotation:** 6500 rpm
- **Air velocity:** 0.1 m/s
- **Gravity** 9.81 $\mathrm{m/s^2}$
- **Time:** Transient
- **Time step size:** 0.15
- **Number of time step:** 26
- **Number of iteration per step:** 100
- **Viscous model:** K-Epsilon (realizable)
- **Near wall treatment:** Scalable wall function
- **Flying medium:** Air
- **Specified operating density:** 1.225 $\mathrm{kg/m^3}$

Ice Formation Simulation Settings:

- **Air velocity:** 0.1 m/s
- **Air static pressure:** 101325 Pa
- **Air static temperature:** 268.15 K

- **Rotating speed:** 6500 rpm
- **Maximum number of time steps:** 100–120
- **Roughness type and height:** Specific sand grain, 0.00005 m
- **CFL number:** 20

Methodology: Ansys Fluent and FENSAP-ICE was used for the calculation of thrust and accumulation of ice in regular and bio inspired propeller. ANSYS Fluent was used to simulate airflow and thrust generation based on the methodology described in "Flow and Structural Analysis of a Quadcopter UAV" [20]. The CFD model employed transient conditions with appropriate inlet velocities, turbulence models, and boundary definitions to capture pressure, velocity, and thrust distribution over the propeller blades. This allowed accurate estimation of aerodynamic efficiency and the effect of blade geometry on performance.

For icing simulations, ANSYS FENSAP-ICE was used. The module integrates with Fluent to simulate droplet trajectories, impingement rates, freezing fractions, and ice accretion. Aerodynamic flow field was first created and then thermodynamic and particle-tracking calculations determined the ice thickness and other parameters. The simulations also included surface roughness to represent penguin-feather-like surfaces, aimed at reducing ice adhesion.

6 Acknowledgements

We acknowledge the open data and manufacturer resources listed in the References for providing technical specifications used in the parameter table. Computational analyses used Google Colab(Python) and ANSYS Workbench; the corresponding notebooks and project files are provided. We also acknowledge the use of AI-assisted tools solely for structuring, formatting, and code debugging support. No scientific analysis, interpretation, or modeling was performed by AI. All conceptual design, research, simulations, and conclusions were independently conducted and verified by the authors.

References

[1] DNK Power. 18650 battery pack calculator. https://www.dnkpower.com/18650-battery-pack-calculator/, 2024. Accessed 2025-10.

[2] BatteryDesign.net. Specific heat capacity of lithium-ion cells. https://www.batterydesign.net/specific-heat-capacity-of-lithium-ion-cells/, 2024. Accessed 2025-10.

[3] Engineering Toolbox. Convective heat transfer coefficients. https://www.engineeringtoolbox.com/convective-heat-transfer-d_430.html, 2024. Accessed 2025-10.

[4] Nuclear Power Encyclopedia. Convective heat transfer coefficient overview. https://www.nuclear-power.com/nuclear-engineering/heat-transfer/convection-convective-heat-transfer/convective-heat-transfer-coefficient/, 2024. Accessed 2025-10.

[5] Image Reference. Convective coefficient reference image. https://ibb.co/q3TxmXqg, 2024. Accessed 2025-10.

[6] Amazon. Battery enclosure (amazon product reference). https://amzn.in/d/bSq7QTt, 2024. Accessed 2025-10.

[7] Ganapathi Pamula and Ashwin Ramachandran. Thermal management for unmanned aerial vehicle payloads: Mechanisms, systems, and applications. *Drones*, 2025.

[8] Science Buddies Staff. How hand warmers work: An experiment on exothermic reactions, 2024. Accessed October 2025.

[9] Rubitherm Technologies GmbH. Rt0 technical datasheet. https://www.rubitherm.eu/media/products/datasheets/Techdata_-RT0_EN_30092020.PDF, 2020.

[10] Federal Aviation Administration. Faa report ar-01-91: Aircraft icing conditions. Technical report, Federal Aviation Administration, 2001.

[11] UCAR SciEd. Cloud droplets and raindrop sizes. https://scied.ucar.edu/image/aerosols-raindrop-cloud-droplets-sizes, 2023.

[12] Michael J. Wood, Gregory Brock, and Anne-Marie Kietzig. The penguin feather as inspiration for anti-icing surfaces. *Cold Regions Science and Technology*, 213:103903, 2023.

[13] Derek Harvey, Eric Villeneuve, Mathieu Béland, and Maxime Lapalme. Wind tunnel investigation of the icing of a drone rotor in forward flight. *Drones*, 8, 2024.

[14] Irving Langmuir and Katharine Blodgett. A mathematical investigation of water droplet trajectories. *Columbia University Press, Meteorological Papers*, 3, 1946.

[15] Michael B. Bragg and Richard J. Kind. Aircraft icing handbook volume i: Effects of ice accretion on aircraft aerodynamics. Technical Report NASA CR-15014, NASA, 1988.

[16] J. R. Buser et al. Precision chemical heating for diagnostic devices. *Lab on a Chip*, 15(1):154–160, 2015. Accessed 2025-10-29.

[17] Linda Wang. What's inside disposable hand warmers? *Chemical Engineering News*, 88(4), 2010. Accessed 2025-10-29.

[18] Shawn P. Scroger, Jose Palacios, and Yiqiang Han. Empirical modeling of urban air mobility rotor icing thrust degradation. In *AIAA Aviation 2020 Forum*, 2020. Accessed 2025-10.

[19] Manaf Muhammed and Muhammad Shakeel Virk. Ice accretion on rotary-wing unmanned aerial vehicles — a review study. *Aerospace*, 10(3):261, 2023. Accessed 2025-10.

[20] Faraz Ahmad, Pushpendra Kumar, Yasar Khan, and Pravin Patil. Flow and structural analysis of a quadcopter uav. pages 880–888, 08 2020.